ORIGINAL PAPER

An empirical theory for gravitationally unstable flow in porous media

R. Farajzadeh · B. Meulenbroek · D. Daniel · A. Riaz · J. Bruining

Abstract In this paper, we follow a similar procedure as proposed by Koval (SPE J 3(2):145–154, 1963) to analytically model CO_2 transfer between the overriding carbon dioxide layer and the brine layer below it. We show that a very thin diffusive layer on top separates the interface from a gravitationally unstable convective flow layer below it. Flow in the gravitationally unstable layer is described by the theory of Koval, a theory that is widely used and which describes miscible displacement as a pseudo two-phase flow problem. The pseudo two-phase flow problem provides the average concentration of CO_2 in the brine as a function of distance. We find that downstream of the diffusive layer, the solution of the convective part of the model, is a rarefaction solution that starts at the saturation corresponding to the highest value of the fractional-flow function. The model uses two free parameters, viz., a dilution factor and a gravity fingering index. A comparison of the Koval model with the horizontally averaged concentrations obtained from 2-D numerical simulations provides a correlation for the two parameters with the Rayleigh number. The obtained scaling relations can be used in numerical simulators to account for the density-driven natural convection, which cannot be currently captured because the grid cells are typically orders of magnitude larger than the wavelength of the initial fingers. The method can be applied both for storage of greenhouse gases in aquifers and for EOR processes using carbon dioxide or other solvents.

Keywords CO_2 sequestration · Density-driven natural convection · Enhanced mass transfer · Analytical modeling

R. Farajzadeh (✉) · B. Meulenbroek · J. Bruining
Delft University of Technology, Delft, The Netherlands
e-mail: r.farajzadeh@tudelft.nl

R. Farajzadeh
Shell Global Solutions International B.V., Rijswijk, The Netherlands

D. Daniel · A. Riaz
University of Maryland, College Park, USA

Nomenclature

C	Dimensionless concentration (dimensionless)
D	Diffusion coefficient (in square meter per second)
E	Effective viscosity ratio
f	Fractional-flow function
g	Acceleration due to gravity (in meter per square second)
H	Height of the porous medium (in meter)
H_k	Koval heterogeneity factor (dimensionless)
J	Convective mass flux (dimensionless)
K	Permeability of the porous medium (in square meter)
k_r	Relative permeability (dimensionless)
K	Koval factor
K_G	Gravity fingering index
m_D	Normalized mass of dissolved CO_2
p	Pressure (in pascal)
Pe	Peclet number (dimensionless)
Ra	Rayleigh number (dimensionless)
S	Phase saturation (dimensionless)
t	Time (in second)
u_c	Dimensionless velocity (dimensionless)
U	Velocity (in meter per second)
V_{DP}	Dykstra–Parsons coefficient

X Rescaled z-coordinate (ξ/ε)
Z Distance in z-coordinate

Greek symbols

α_τ Dilution factor
ϵ 1/Pe
φ Porosity of the porous medium (dimensionless)
h Transformation coordinate
λ_c Wavelength (in meter)
λ Mobility (k_r/μ)
Λ Mobility ratio of phase (dimensionless)
μ Viscosity of the fluid (in kilogram per meter-second)
ξ Dimensionless distance (z/H)
p Density of the fluid (in kilogram per cubic meter)
τ Dimensionless time (dimensionless)

Subscripts

i Initial value of the quantity
m Mixture phase
s Pure solvent
w Water phase
z Quantity in z-direction

1 Introduction

When a denser fluid is placed on top of a lighter one, it can lead to Rayleigh–Taylor instabilities [43]. This phenomenon is of importance for many fields of science and engineering (see, e.g., [42]); however, we confine our interest to CO_2–brine and CO_2–oil systems, relevant for CO_2 sequestration and enhanced oil-recovery processes. The instabilities initiated by local density increase of brine (or oil), caused by dissolution of CO_2, increases the mass-transfer rate of CO_2 in brine (or oil) [10–12, 14, 51]. Even if the same approach can indeed be used for CO_2–oil displacements, this paper entirely focuses on CO_2–water displacement. The increase of the mass-transfer rate is equivalent to a dissolution of a larger amount of CO_2 in a shorter period of time and faster propagation of CO_2 in porous media (aquifers and hydrocarbon reservoirs) [33, 34, 38]. The large volume of dissolved CO_2 remains permanently in the liquid (at least as long as the pressure remains unchanged) and poses no threat of leakage, which is favorable for geological storage of CO_2 [23].

The efficiency of mixing in density-driven natural convection is governed by the Rayleigh number (Ra), which includes the reservoir permeability and the density difference. A stability analysis of the density-driven natural convection in the saturated porous layers indicates that the time required for the initiation of natural convection is proportional to $\sim Ra^{-2}$ and the critical wavelength is proportional to $\sim Ra^{-1}$ Meulenbroek et al. (2012, under review) [39]. The critical wavelength, λ_c, is an indication of the grid size required to capture the initiation of the initial fingers. Let us define Rayleigh number by

$$Ra = \frac{k\Delta\rho g H}{\varphi\mu_w D}. \tag{1}$$

For the values of $k = 1$ Darcy, $\Delta\rho = 10$ kg/m³, $g = 10$ m/s², $H = 50$ m, $\mu_w = 1$ cP, $D = 2 \times 10^{-9}$ m²/s, and $\varphi = 0.2$, we obtain Ra $= 1.25 \times 10^4$, which using the analysis of Meulenbroek et al. (2012, under review) provides $\lambda_c = 110\ H\ /$ Ra $\sim 0.009\ H = 50$ cm. This implies that accurate estimation of the amount of dissolved CO_2 in brine under these conditions requires grid sizes much smaller than 50 cm. For highly permeable and heterogeneous porous media, the required grid size may be too small to resolve even with massively parallel architectures [32, 34]. This necessitates the development of simpler models that could approximately quantify the amount of dissolved CO_2 after the injection period taking into account the instabilities.

In miscible displacement, the viscosity difference between the solvent and the oil leads to development of fingers that adversely affects the oil recovery. The characteristic fingering behavior of the solvent concentration profile cannot be predicted by fractional-flow-based miscible displacement models, originally described by [35]. Koval [28] developed a simple model to account for the instabilities (fingering behavior) observed in the miscible displacements. The significance of Koval theory, which has become a standard for representing instabilities in miscible displacements in the petroleum industry, apart from its simplicity, is because of the fact that it is able to reproduce the experimental data in a horizontal configuration very well [47]. In this model, the viscosity ratio between the displacing and displaced fluids in the fractional-flow function of the Buckley–Leverett equation, which is defined as

$$f_{BL}(S) = \frac{1}{1 + \frac{k_{ro}(S)}{k_{rs}(S)}\frac{\mu_s}{\mu_o}}, \tag{2a}$$

is replaced by the Koval factor, K.

Therefore, in Koval's model, Eq. 2a becomes

$$f_{koval}(S) = \frac{1}{1 + \frac{1-S}{S}\frac{1}{K}}, \tag{2b}$$

where we also note that Koval uses S to denote a concentration, as his inspiration comes from the description of oil–water flow, where S is used as the saturation.

Indeed, k_{ro} is the relative permeability of the displaced fluid (i.e., oil), k_{rs} is the relative permeability of the displacing fluid (i.e., the mixture of solvent and the oil) that now has been assumed to be a linear function of its saturation, μ_o is the oil viscosity, μ_s is the solvent viscosity, and the Koval factor is given by $K = H_k E$. Here, E is the "effective" viscosity ratio and is defined as the ratio between the oil viscosity and the viscosity of the mixture of oil and solvent in which the volume fraction of the solvent is S_e. The effective viscosity of the displacing fluid can be calculated from the "1/4 power" mixing rule:

$$E = \left((1 - S_e) + S_e \left(\mu_o/\mu_s\right)^{1/4}\right)^4.$$

E is chosen such that the results of the model fit the experimental data. Using the experiments of [3], Koval found that $S_e = 0.22$, i.e., the mixture of solvent and oil that displaces the oil contains 22 % solvent [28].

In spite of its success, Koval's model cannot be used for all miscible displacement problems. [4, 5] shows that Koval is only performing well for high Peclet number conditions and sees no easy method to extend the theory to low Peclet number conditions. The Peclet number describes the ratio of convective transport and diffusion transport and is in the vertical setting similar to the Rayleigh number (Eq. 1). Yortsos and Salin [52] derive bounds to show that the mixing zone develops much slower than given by the "naïve solution of transverse averaged equations."

However, numerical simulations of [5] suggest that taking $S_e = 0.22$ gives good agreement between Koval's theory and numerical simulations at high Peclet numbers. For heterogeneous reservoirs, E is multiplied by the Koval heterogeneity index, H_k, which is related to the Dykstra–Parsons coefficient by [30]

$$\log H_k = \frac{V_{DP}}{(1 - V_{DP})^{0.2}}. \tag{3}$$

The degree of heterogeneity of the permeability field determines the character of the density-driven natural convection flow in porous media. Similar to the instabilities induced by the viscosity difference between the fluids [47], instabilities induced by a density difference can lead to *f*ingering, *c*hanneling, and dispersive regimes depending on the degree of the permeability variance (Dykstra–Parsons coefficient) and the correlation length of the porous medium [15, 37]. The dispersive regime (characteristic of flow in media with a high degree of heterogeneity) can be analytically modeled

by choosing an effective dispersion coefficient in a diffusion-based model [20]. In the channeling regime, which occurs for a medium degree of heterogeneity, there is no correlation with the measures of heterogeneity and the transfer rate of CO_2 in water, and therefore, the method proposed by Koval cannot be applied without modification. Here, we confine our interest to finding an analytical model for a low degree of heterogeneity, which leads to a fingering regime. It could be validated that for a low degree of heterogeneity, the effect of heterogeneity on the transfer rate is relatively small.

This paper concerns the use of Koval's theory to describe gravity-induced fingering. Unfortunately, Koval is not performing as well for gravity-induced instabilities as for horizontal unstable flow. There are many experimental studies on viscous fingering with gravity effects, e.g., [3, 22, 26, 50]. When used to test the theory, they all give less accurate results than for horizontal flow. Dougherty [8] extended the Koval model to include gravity. He discussed various expressions for the driving force to optimize agreement with experimental results of [3]. Fayers and Newley [18] and [17] introduced a three-parameter model to obtain a better description of viscous fingering with gravity effects. However, [19] pointed to the poor performance for gravity flow indicated, not only for Koval model itself but also for extensions like the [17, 44] models.

In spite of this and in view of the fact that the Koval model is well representing the qualitative features of unstable miscible flow, we will use it as a starting point for developing the theory below. We do not attempt to include saturation dependences of the density and viscosity [8, 36], as this deserves a separate study. We show that including a diffusion coefficient will both describe the diffusive layer near the entrance as the unstable behavior away from the interface.

Therefore, the objective of this paper is to develop an analytical model that predicts the performance of gravitationally unstable flow in porous media. Our special focus will be on the inclusion of the effect of fingering on the transfer rate of CO_2 in brine. As indicated above, we use an analogous procedure as proposed by [28]. The proposed model is similar to the Buckley–Leverett method for gravity-dominated flow. The flow function uses the dilution parameter α_τ and a "gravity fingering index" as an input (K_G factor). The solution provides the average concentration of CO_2 in the brine as a function of distance and eventually the total mass of dissolved CO_2. The structure of the paper is as follows: First, we describe the physical model and provide the ensuing equations. Next, we use the method of matched asymptotic expansions to obtain an approx-

imate analytical solution for the described equations. Afterwards, we introduce empirical parameters into the model to take into account the fingering behavior and compare the results of the proposed model to the numerical simulations. Finally, we draw the main conclusions of this study.

2 Physical model

Figure 1 schematically shows the purpose of the model, i.e., to capture the averaged behavior of the process in the direction of the flow. If there is no instability, there will be a short transition zone (here, the ensuing error function is represented as a shock) between the CO_2-containing brine at the top and the initial brine that contains no CO_2. This occurs when the flow regime is diffusive (e.g., at the initial stages of the process) or dispersive (for highly heterogeneous media). This behavior can be accurately modeled through diffusion-based models, albeit with an effective diffusion coefficient. When instabilities occur, the concentration front moves faster and there is a gradual change from a high (horizontally averaged) concentration of CO_2 at the top to the initial concentration.

2.1 Formulation

We consider a 1-D porous medium of length H that is initially saturated with water. The vertical coordinate, z, is taken positive in the downward direction. The constant porosity of the porous medium is φ and its permeability is k. Initially, there is no CO_2 dissolved in water ($S_i = 0$). We assume a no-flow boundary at the bottom of the porous medium. CO_2 is continuously supplied from the top, i.e., the CO_2 concentration at the top is kept constant and therefore the water at the interface is fully saturated with CO_2. We consider the water and water saturated with CO_2 (referred to as "mixture" and represented by m) as two separate phases: (1) pure water with density ρ_w and viscosity μ_w

and (2) a mixture phase that contains two components, i.e., CO_2 and water with density ρ_m and viscosity μ_m. We disregard the presence of a capillary transition zone between water and mixture phases and assume that the relative permeability of the mixture is proportional to its saturation denoted by S_m. In the same way, the relative permeability of the water phase is proportional to its saturation $S_w = 1 - S_m$. The saturation of the mixture can be interpreted as the local concentration of the solvent at the respective time and point in the space, i.e., $S(z,t)$.

2.2 Governing equations

The motion of fluids in a porous medium can be described by Darcy's law. The Darcy equation for the mixture can be written as

$$u_m = -\lambda_m \left(\frac{\partial p_m}{\partial z} - \rho_m g \right). \tag{4}$$

The Darcy equation for water reads

$$u_w = -\lambda_w \left(\frac{\partial p_w}{\partial z} - \rho_w g \right), \tag{5}$$

where u is the Darcy velocity, p_α ($\alpha = m, w$) is the pressure of phase α, ρ_α is the density of phase α, g is the acceleration due to gravity, and $\lambda_\alpha = k k_{r\alpha} / \mu_\alpha$ ($\alpha = m, w$) is the mobility, which is the ratio between the phase permeability $k k_{r\alpha}$ and the viscosity μ_α. Subscripts m and w denote the $CO_2 +$ water mixture and the initial water, respectively. Both viscosity [1, 29] and density [9, 25] are functions of the CO_2 concentration and increase with increasing carbon dioxide concentration. The pressure in both phases is the same as we ignore the capillary forces and therefore $p_m = p_w = p$.

The saturated density difference between an aqueous solution of CO_2 and pure water is given by $c_\rho p_g$, where the value of the $c_\rho = 0.261$ kg/m³/bar for pure water (see [21], p. 72); c_ρ will be less for formation brines, because the solubility of CO_2 in water decreases with increasing salinity. Therefore, the density of the

Fig. 1 Schematic of **a** stable and **b** unstable displacement and transverse average of the corresponding concentration profiles
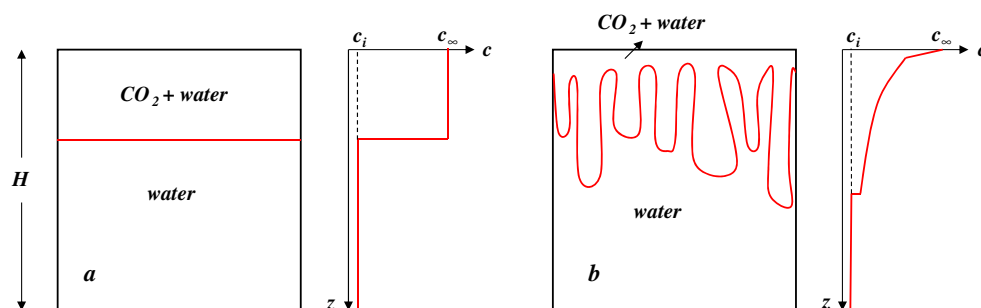
mixture can be assumed to increase according to the following relationship:

$$\Delta \rho = \rho_m - \rho_w = \alpha_\tau \left(c_\rho \, p_g \right) = \alpha_\tau \Delta \rho_{\mathrm{max}}., \tag{6}$$

$\Delta \rho_{\mathrm{max}}$ will only be established at the beginning of the process when the interface is fully saturated with CO_2 and the underlying liquid contains no CO_2. When the instabilities initiate, $\Delta \rho$ or the driving force at the front is the density difference between the brine–CO_2 mixture at the tip of advancing fingers and the initial brine. However, as the CO_2 fingers move away from the interface, the concentration of CO_2 in the fingers decreases. To account for these effects, $\Delta \rho_{\mathrm{max}}$ is multiplied by a "dilution factor" α_τ, whose value decreases with increasing Rayleigh number. Taking α_τ as constant for each Rayleigh number implies that the mass transfer is proportional to time. It turns out that this is true until the transient Sherwood number (the history of the ratio between the cumulative mass of the CO_2 transported to the liquid by convection and diffusion and the cumulative mass transported in the absence of convection) reaches its maximum value. Indeed, the experimental results indicate that initially the mass transfer of CO_2 into water increases significantly by convection until the transient Sherwood number reaches a maximum, and afterwards, it starts to decrease due to the decreasing importance of natural convection effects when the CO_2 becomes distributed more evenly [14]. The maximum transient Sherwood number occurs when CO_2 reaches the bottom of the porous medium and the mass transfer is no longer linear with time; therefore, the time dependency of α_τ should be considered only after this time.

We assume ideal mixing and use the Boussinesq approximation, i.e., we only consider the density variations in Eqs. 4 and 5. With this assumption and because there is no source or sink in our model, the volume conservation is equivalent to mass conservation and therefore

$$u_m + u_w = 0, \tag{7}$$

which implies a countercurrent flow. We can derive an expression for the Darcy velocity of the mixture, i.e.,

$$u_m + u_w = 0 = u_m - \frac{\lambda_w}{\lambda_m} \lambda_m \left(\frac{\partial p}{\partial z} - \rho_m g \right) - \lambda_w \left(\rho_m - \rho_w \right) g. \tag{8}$$

We replace the term containing the expression $(\partial p / \partial z - \rho_m g)$ by $u_m \lambda_w / \lambda_m$ and it follows that

$$u_m = \frac{\lambda_w \lambda_m}{\lambda_w + \lambda_m} \left(\rho_m - \rho_w \right) g. \tag{9}$$

The conservation law for the mixture including diffusion reads

$$\varphi \frac{\partial S_m}{\partial t} + \frac{\partial u_m}{\partial z} = \varphi D \frac{\partial^2 S_m}{\partial z^2}. \tag{10}$$

Substitution of Eq. 9 into Eq. 10 leads to

$$\varphi \frac{\partial S_m}{\partial t} + \frac{\partial}{\partial z} \left(\frac{\lambda_w \lambda_m}{\lambda_w + \lambda_m} \left(\rho_m - \rho_w \right) g \right) = \varphi D \frac{\partial^2 S_m}{\partial z^2}. \tag{11}$$

2.3 Dimensionless form of the equations

We scale the velocity with a reference velocity $u_c = k \Delta \rho_{\mathrm{max}} g / \mu_w$, the length with $H_{,,}$ and t with $\varphi H / \mu_c$. Therefore, Eq. 11 now reads

$$\frac{\partial S_m}{\partial \tau} + \frac{\partial}{\partial \xi} \left(\frac{\alpha_\tau k_{\mathrm{rw}}}{1 + \Lambda^{-1}} \right) = \varepsilon \frac{\partial^2 S_m}{\partial \xi^2}, \tag{12}$$

where $\tau = (\mu_c / \varphi H) \, t$, $\xi = z / H$, $\Lambda = \lambda_m / \lambda_w$, $\varepsilon = 1 / Pe$, and $Pe = u_c H / \varphi D = Ra$. We define the "fractional-flow function" as

$$f(S_m) = \frac{k_{\mathrm{rw}}}{1 + \Lambda^{-1}}. \tag{13}$$

Therefore, Eq. 12 can be written as

$$\frac{1}{\alpha_\tau} \frac{\partial S_m}{\partial \tau} + \frac{df(S_m)}{dS_m} \frac{\partial S_m}{\partial \xi} = \frac{\varepsilon}{\alpha_\tau} \frac{\partial^2 S_m}{\partial \xi^2}, \tag{14}$$

as α_τ is considered constant. The Peclet number, Pe, is defined as the ratio between the convective and diffusive fluxes. For the values mentioned earlier, we will obtain $u_c = 2 \times 10^{-7}$ m/s. Using $D = 2 \times 10^{-9}$ m^2/s, we obtain Pe = 5,000. Zimmerman and Homsy [53] noted that for Pe $>> 1$, it is reasonable to model the diffusion as constant and isotropic because at large Peclet numbers, all averaged quantities are independent of any anisotropy (see also [5]). Therefore taking D as constant is justified. We notice that for very large Peclet numbers (Pe$\to \infty$ or $\varepsilon \to 0$), Eq. 14 converts to the classical Buckley–Leverett type of equation, albeit with a different fractional-flow function.

In the displacement problems, the initiation of the flow is forced by injection. In our case, the flow rate cannot be forced. Therefore, a crucial parameter of the model is to define the top boundary condition. If we assume that the saturation of the mixture is 1, it is not immediately clear how unstable convective motion would initiate. Here, we will investigate the approximate analytical solution of Eq. 14 with the method of matched asymptotic expansions [45] and compare it with the numerical solution.

2.4 Approximate solutions

The approximate solution consists of an inner solution in the domain $R_1 = [0, \varepsilon)$, where diffusion dominates, and an outer solution in $R_2 = (\varepsilon, 1]$ that is convection-dominated. This behavior is also shown experimentally [27]. It turns out that the outer solution consists of a rarefaction solution and that the inner solution concerns the stationary diffusion equation.

2.4.1 Rarefaction (or outer) solutions

In the absence of diffusion, the solution consists of rarefactions and constant states. The rarefaction solution will be followed by a shock if the $\Delta \rho_{\max}$ in Eq. 6 is assumed to be a function of saturation [16]. In the following, we derive the rarefaction solution and the constant state. We can use a coordinate transformation $\eta = \xi / (\alpha_\tau \tau)$ and obtain from Eq. 14

$$\left(-\eta + \frac{df \left(S_{\mathrm{m}}^{\mathrm{out}} \right)}{dS_{\mathrm{m}}^{\mathrm{out}}} \right) \frac{dS_{\mathrm{m}}^{\mathrm{out}}}{d\eta} = 0. \tag{15}$$

where the superscript "out" refers to the outer solution. The value of α_τ only changes the meaning of η in the sense that the same "outer" profile is obtained after τ / α_τ with respect to the case with $\alpha_\tau = 1$. The inner profile, which is governed by the equation

$$\frac{df \left(S_{\mathrm{m}}^{\mathrm{in}} \right)}{dS_{\mathrm{m}}^{\mathrm{in}}} \frac{\partial S_{\mathrm{m}}^{\mathrm{in}}}{\partial \xi} = \frac{\varepsilon}{\alpha_\tau} \frac{\partial^2 S_{\mathrm{m}}^{\mathrm{in}}}{\partial \xi^2},$$

is affected by the value of α_τ in a different way. This means that the outer and inner solutions use a different scaling factor. However, in the comparisons below (Figs. 5, 6, 7 and 8), we will not use the inner solution (see Eq. 28) and we will only show the outer solution.
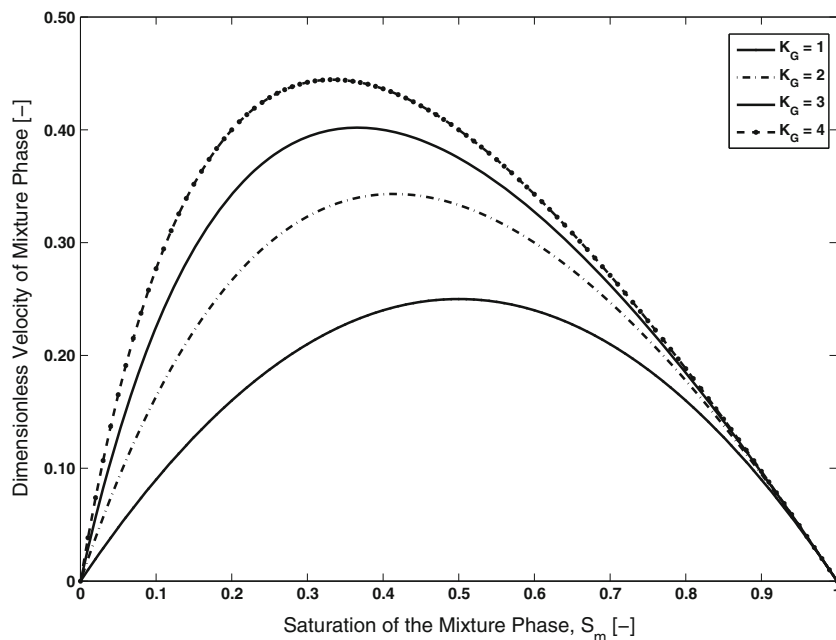
The solution of Eq. 15 is either a constant state $dS_{\mathrm{m}}^{\mathrm{out}}/d\eta = 0$ or

$$\eta = \frac{df \left(dS_{\mathrm{m}}^{\mathrm{out}} \right)}{dS_{\mathrm{m}}^{\mathrm{out}}}. \tag{16}$$

In the rest of this section, we omit the superscript out to avoid cumbersome notation. Equation 16 can be solved to obtain $S_{\mathrm{m}} = S_{\mathrm{m}}(\eta)$ on condition that the second derivative of the fractional-flow function does not change sign [31, 41], i.e., in the absence of shocks. Replacing $k_{\mathrm{rw}} = (1 - S_{\mathrm{in}})$, $\lambda_{\mathrm{m}} = k S_{\mathrm{in}} / \mu_{\mathrm{m}}$, $\lambda_{\mathrm{w}} = k(1 - S_{\mathrm{in}})/\mu_{\mathrm{w}}$ in Eq. 13, we obtain

$$\eta = \frac{d}{dS_{\mathrm{m}}} \left(\frac{(1 - S_{\mathrm{m}})}{\frac{(1-S_{\mathrm{m}})}{S_{\mathrm{m}}} \frac{1}{K_{\mathrm{G}}} + 1} \right), \tag{17}$$

where we have replaced $\mu_{\mathrm{w}} / \mu_{\mathrm{m}}$ with K_{G} similar to Koval's fractional-flow function in Eq. 2b. As already indicated above, this choice of linear relative permeabilities was introduced by Koval to describe miscible displacement. The introduction of the K_{G} factor is equivalent to scaling of the relative permeability of the mixture phase by a factor K_{G} and keeping the viscosity ratio in the equation (which is very close to unity). The latter is similar to the pseudo relative permeability approach that is a well-accepted approach of up-scaling in the petroleum engineering literature [6, 7, 24, 49]. The

Fig. 2 Plot of dimensionless phase velocity, i.e., term in brackets in RHS of Eq. 17 versus saturation. Just downstream of the diffusion layer, all solutions start at the saturation corresponding to the highest phase velocity with a rarefaction

term in brackets is plotted in Fig. 2 for different values of K_G. We note that experimental data suggest that $\mu_m > \mu_w$, which would lead to $K_G < 1$. In other words, we attribute nonphysical values to K_G. Downstream of the diffusive layer, the solution of Eq. 17 for different values of K_G starts at the saturation corresponding to the highest phase velocity (maximum of the fraction-flow function) with a rarefaction solution. We refer to K_G as the gravity fingering index and use it as a fitting parameter to obtain agreement between the numerical and analytical results. The general rarefaction solution of Eq. 17 is

$$\eta = -\frac{S_m K_G}{1 + S_m (K_G - 1)} + \frac{K_G (1 - S_m)}{(1 + S_m (K_G - 1))^2}. \tag{18}$$

For $K_G = 1$, i.e., $\mu_m = \mu_w$, the solution is simplified to

$$\eta = (1 - 2S_m). \tag{19}$$

2.4.2 Diffusion equation (or inner) solution

In R_1, we rescale the z-coordinate $X = \frac{\alpha_\tau \xi}{\varepsilon}$ in Eq. 12. This leads to

$$\varepsilon \frac{\partial S_m^{in}}{\partial \tau} + \frac{\partial f\left(S_m^{in}\right)}{\partial X} = \frac{\partial^2 S_m^{in}}{\partial X^2}. \tag{20}$$

where the superscript "in" refers to the inner solution. The first term on the left-hand side of Eq. 20 is small with respect to the other terms and can be omitted. Then, Eq. 20 becomes

$$\frac{\partial f\left(S_m^{in}\right)}{\partial X} = \frac{\partial^2 S_m^{in}}{\partial X^2}. \tag{21}$$

Integration of Eq. 21 gives

$$\frac{\partial S_m^{in}}{\partial X} = f\left(S_m^{in}\right) + \delta, \tag{22}$$

where δ is a constant. The matching condition reads [45, 46]

$$\lim_{X \to \infty} S_m^{in}(X) = \lim_{\xi \to 0} S_m^{out}(\xi) = S_m^0.$$

From Eq. 18, we have

$$\eta = 0 \Rightarrow S_m^0 = \frac{1}{1 + \sqrt{K_G}}. \tag{23}$$

S_m^0 is the saturation that separates the diffusive and rarefaction regimes. Notice that this is the saturation where the fractional-flow function attains its maximum. The second boundary for Eq. 21 reads $S_m^0(0) = 1$.

Defining a new integration constant $\kappa = \delta/K_G$ instead of δ and using Eqs. 13, 17, and 22, we obtain

$$\frac{dS_m^{in}}{dX} = f\left(S_m^{in}\right) + \kappa K_G$$

$$= K_G \left(\frac{(1 - S_m^{in}) S_m^{in} + \kappa (1 - S_m^{in}(1 - K_G))}{1 - S_m^{in}(1 - K_G)}\right). \tag{24}$$

As $X \to \infty$, we know that $S_m^{in} \to S_m^0$, which means that $dS_m^{in}/dX \to 0$ as $X \to \infty$, and therefore, $dS_m^{in}/dX \to 0$ as $S_m^{in} \to S_m^0$. Therefore, the numerator in Eq. 24 must be proportional to $S_m^{in} \to S_m^0$, and since the numerator is quadratic in S_m^{in}, we find

$$\left(1 - S_m^{in}\right) S_m^{in} + \kappa \left(1 - S_m^{in}(1 - K_G)\right)$$
$$= -\left(S_m^{in} - S_m^0\right)\left(S_m^{in} - \gamma\right) \tag{25}$$

from which we find

$$\gamma = \frac{S_m^0 - 1}{S_m^0 - K_G S_m^0 - 1}. \tag{26}$$

Combining Eqs. 23 and 26, we obtain

$$\gamma = S_m^0. \tag{27}$$

Substitution of Eq. 27 into Eq. 24 and integration gives

$$\int \frac{1 - S_m^{in}(1 - K_G)}{\left(S_m^{in} - S_m^0\right)^2}$$

$$dS_m^{in} = \int \frac{-(1 - K_G)\left(S_m^{in} - S_m^0\right) + 1 - S_m^0(1 - K_G)}{\left(S_m^{in} - S_m^0\right)^2}$$

$$dS_m^{in} = -K_G X + C,$$

and we obtain

$$-K_G X + C = -(1 - K_G) \ln\left(S_m^{in} - S_m^0\right)$$
$$-\frac{1 - S_m^0(1 - K_G)}{S_m^{in} - S_m^0} = \frac{2S_m^0 - 1}{\left(S_m^0\right)^2} \ln\left(S_m^{in} - S_m^0\right)$$
$$-\frac{1}{S_m^0}\frac{1 - S_m^0}{\left(S_m^{in} - S_m^0\right)},$$

where we used Eq. 23 to replace K_G by $\left(\frac{1}{S_m^0} - 1\right)^2$. Using the top boundary condition $S_m^{in}(0) = 1$ at $X = 0$, the numerical constant C can be computed and we obtain

$$-K_G X = \frac{2S_m^0 - 1}{\left(S_m^0\right)^2} \ln\left(\frac{S_m^{in} - S_m^0}{1 - S_m^0}\right) + \frac{1}{S_m^0}\frac{S_m^{in} - 1}{S_m^{in} - S_m^0}. \tag{28}$$

Figure 3 plots the inner solution (Eq. 28) and outer solution (Eq. 19) of this case and compares it to the numerical solution.

Fig. 3 Inner solution (Eq. 28) (dotted curve), outer solution (Eq. 19) (dashed-dotted curve), and numerical solution of Eq. 12 (drawn curve) for Pe = 5,000, $\alpha_\tau = 1$, and $K_G = 1$. Here, we show the solution at breakthrough time τ_{bt} ($\alpha_\tau = 1$). For $\alpha_\tau < 1$, a different solution is obtained and breakthrough occurs at a later time, i.e., τ_{bt} ($\alpha_\tau < 1$) = τ_{bt} ($\alpha_\tau = 1$) / α_τ. The outer coordinate is affected in a different way by α_τ than the inner solution. Below, in Figs. 5, 6, 7 and 8, we will only show the outer solution.
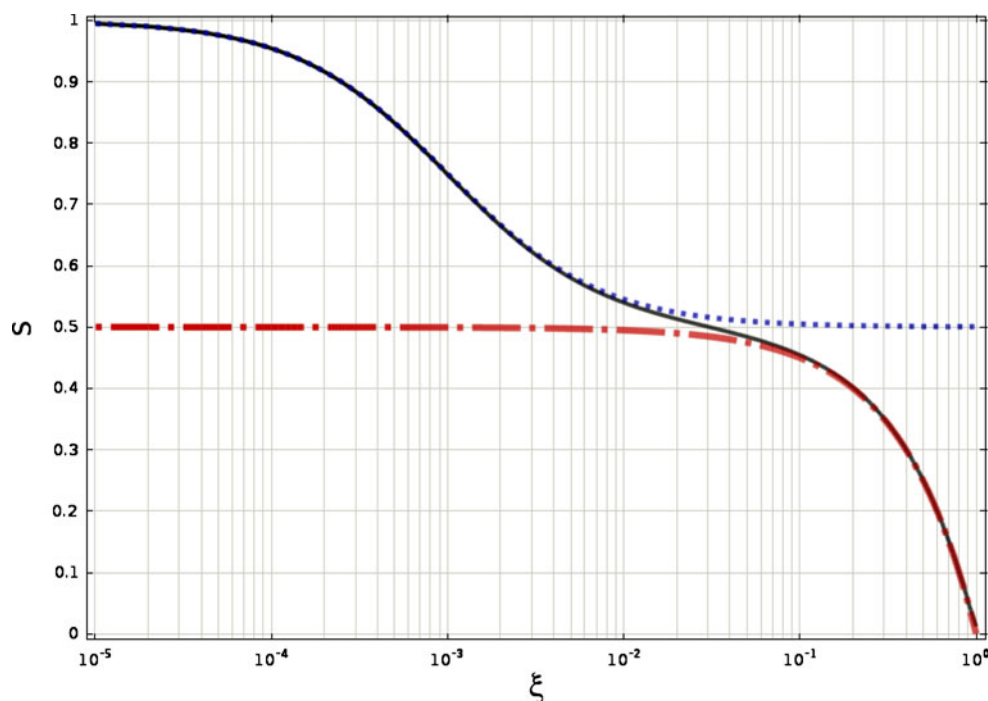
3 Results and discussion

In this section, we present the results of the 1-D analytical model and compare them to the results of the numerical simulations, which were performed in a 2-D porous medium with an aspect ratio (length/width ratio) of 1. A no-flow boundary condition was used at the sides and at the bottom of the medium. The concentration of CO_2 at the top of the medium was assumed to be 1. The initial white noise perturbations are applied within the diffusive layer to reduce the time for the onset of gravity fingering. As seen in [39], perturbations are subjected to high damping till a critical time is reached. Any natural disturbances that occur in the system at early times will be damped significantly. So we look at perturbations at times closer to the critical time. The numerical simulation consists of 512 × 512 grid cells for Ra = 1,000 and 1,024 × 1,024 for Ra > 1,000. The details of the numerical simulations can be found in [39]. We use the same dimensionless numbers as in Section 2.3.

To compare the results, the concentration values of the 2-D numerical simulations were averaged in the horizontal direction. An example is shown in Fig. 4.

Figures 5, 6, 7 and 8 demonstrate the concentration profiles of CO_2 at different times for different Rayleigh numbers. The solid and dashed lines are the results of the 1-D analytical model and the 2-D numerical simulations, respectively. There is qualitative agreement between the two models as to the outer part of the solution, which is all that can be expected for a gravity unstable process [19]. The inner solution is shown in Fig. 3, but not in Figs. 5, 6, 7 and 8 because the solution near the interface (the inner solution) does not affect the transfer rate from the gas to the liquid phase. It describes the steep transition between the surface and asymptotic saturation value S_m near $z = 0$. Figure 3 shows asymptotic saturation value S_m near $z = 0$. For the gravity fingering index $K_G = 1$, the asymptotic saturation value is 0.5 (see Eq. 23). However, the horizontally averaged concentrations obtained from 2-D numerical simulations converge at a smaller value than this saturation value. The saturation value decreases further with increasing Rayleigh number. The value decreases to even smaller values as time progresses, especially for smaller Rayleigh numbers [4]. Therefore, to obtain a reasonable match between the outer analytical and numerical models, the K_G factor was modified such that the asymptotic values of the saturation values S_m near the interface of the two models matched. We ignored time dependency of this value, i.e., we kept the K_G factor independent of time. The fitting parameters of the model, i.e., K_G and α_τ, are listed in Table 1. The K_G factor increases with increasing Rayleigh number, while the dilution factor, α_τ, decreases with increasing Rayleigh number, because as the Rayleigh number increases, the fingers move away faster from the interface.

Note that our model is only valid until CO_2 reaches the bottom of the medium. After this time, CO_2-
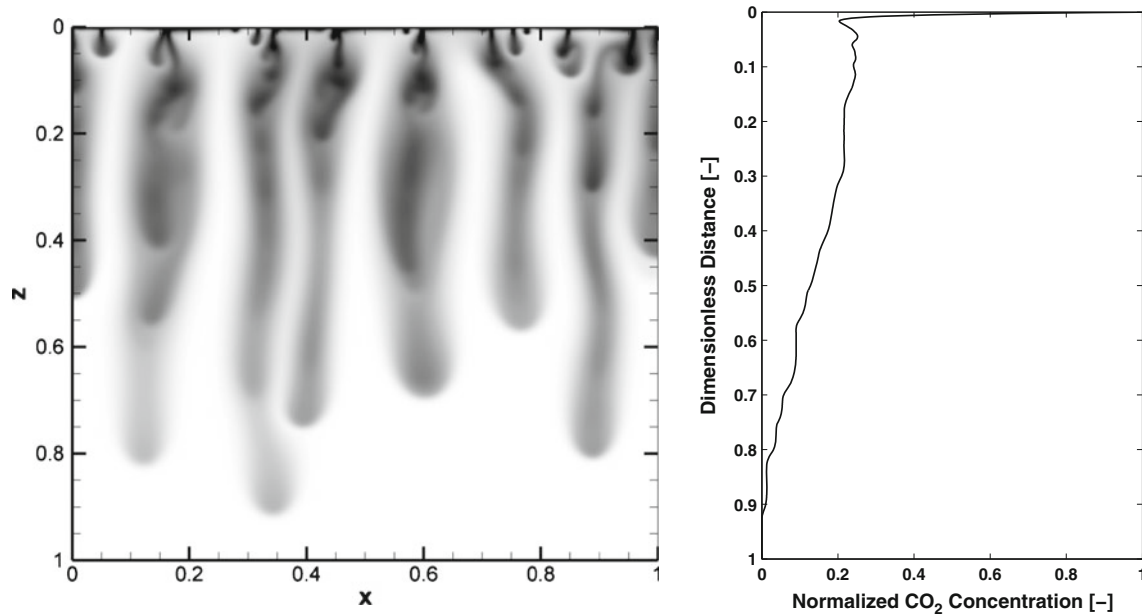
Fig. 4 The concentration profile of CO_2 for Ra = 8,000 at $\tau = 7$. The *right* plot is obtained by averaging the concentration values of the *left* plot in the horizontal direction

saturated solution will start to fill up the layer from the bottom. This filling up was treated in a pioneering paper of [40] and later by [2], who addressed an analogous problem concerning the secondary migration of oil. Oil was moving through countercurrent gravity drainage from the source rock to the future reservoir initially filled with water. The problem is almost the same as the problem considered here except that the saturation exponents of the relative permeabilities are not one for the true two-phase (oil and water) conditions and the trivial fact that the gravity is pointing in the opposite
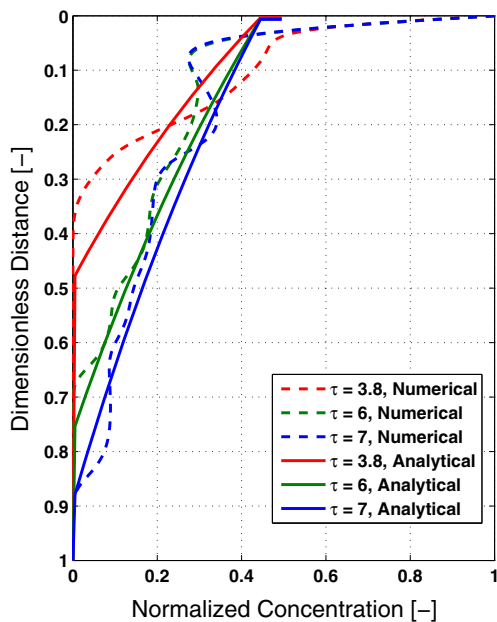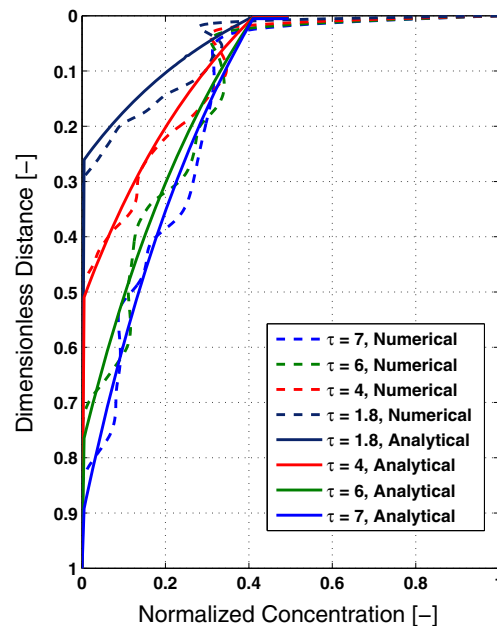

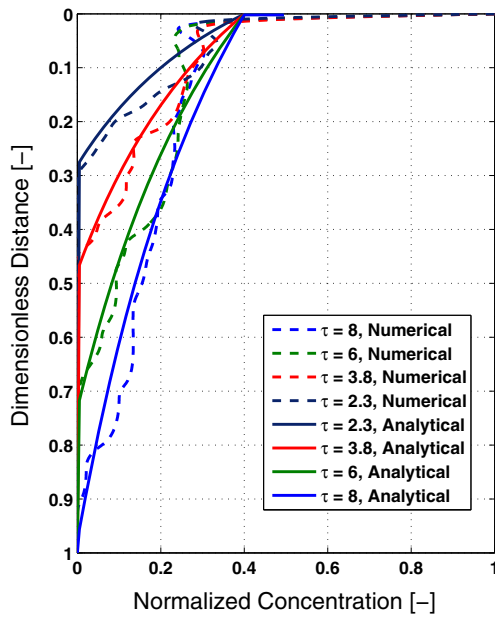**Fig. 5** Comparison between the analytical (solid lines, $K_G = 1.5$, $\alpha_\tau = 0.085$) and numerical (dashed lines) models at different times for Ra = 1,000. The outer analytical solution is obtained by optimizing K_G and α_τ as fitting parameters in Eq. 18. The inner analytical solution (Eq. 28) is not shown in Figs. 5, 6, 7 and 8

Fig. 6 Comparison between the analytical (solid lines, $K_G = 2.0$, $\alpha_\tau = 0.065$) and numerical (dashed lines) models at different times for Ra = 2,000

Fig. 7 Comparison between the analytical (solid lines, $K_G = 2.2$, $\alpha_\tau = 0.055$) and numerical (dashed lines) models at different times for Ra = 4,000

Table 1 The values of K_G and α_τ used as fitting parameters to obtain the "match" between the analytical and numerical models

Rayleigh number	α_τ	K_G
1,000	0.085	1.5
2,000	0.065	2.0
4,000	0.055	2.2
8,000	0.048	2.5

in the paper by [40]. In our case, we assumed a no-flow boundary at the bottom.

By analogy with the Siddiqui–Lake paper, we expect that a reflected wave will occur once the CO_2-saturated solution hits the bottom of the reservoir. Indeed, the saturation of the carbon dioxide-containing aqueous phase near the bottom will increase until it is on the right side $(u_m, S_m) = (0,1)$ in Fig. 2. Here, the wave velocity (see Eq. 17) will be negative (reflected wave). Consequently, the reservoir will stably fill up from the bottom with the saturated solution. Mixed convection and diffusion, and at later stages pure diffusion, will be the dominant mechanisms of this process. To mimic this behavior, α_τ in our model should be assumed time dependent after CO_2 reaches the bottom as mentioned earlier. This aspect will be left for future work.

Figure 9 plots the parameters reported in Table 1 as a function of Rayleigh number. A fitting exercise provides the following relationships:

$$K_G = 0.309 Ra^{0.236}, \quad \alpha_\tau = 0.534 Ra^{-0.271}. \qquad (29)$$

These empirical relations can be used to "effectively" model the gravity-induced instabilities.

Figure 10 plots the mass of the dissolved CO_2 (normalized to the maximum mass that can be dissolved, i.e., m_{sat}) for different Rayleigh numbers and
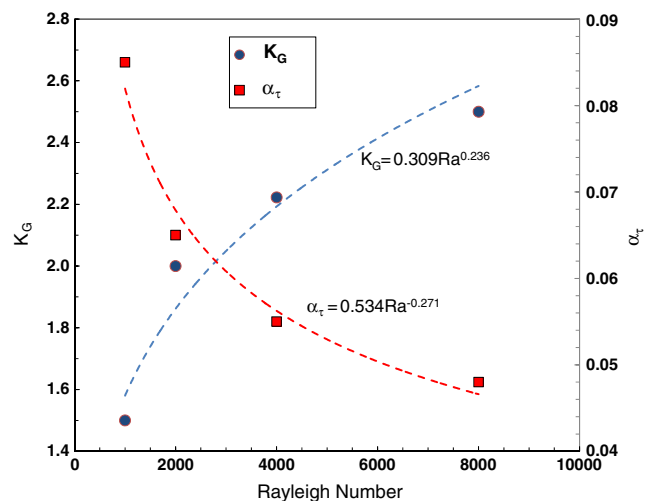
direction. Another main difference is that in the migration problem, the upstream boundary condition (in the source rock) is that the oil saturation is a given low value and is not governed by a diffusion process like here. Downstream there is a seal, which may be partially leaking, which is one of the complicating factors

Fig. 8 Concentration profiles obtained from the analytical (solid lines, $K_G = 2.5$, $\alpha_\tau = 0.048$) and numerical (dashed lines) models at different times for Ra = 8,000

Fig. 9 The fitting parameters as a function of Rayleigh number

Fig. 10 The dimensionless mass of CO_2 dissolved in water obtained from the analytical (solid lines) and numerical (dashed lines) models at different times for different Rayleigh numbers
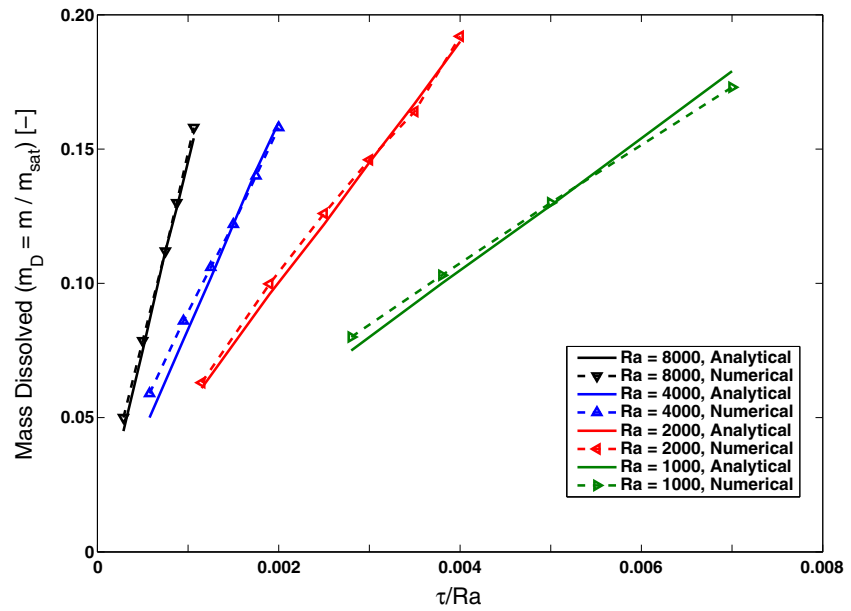
compares it to the numerical model. For illustration purposes, the time has been divided to the corresponding Rayleigh number of each case. A good agreement between the results of the two models is observed if our interest is only in the transfer rate between the gas phase and the liquid phase. The agreement only requires two parameters as a function of the Rayleigh number.

We observe from Fig. 10 that the slope of the lines increases as the Rayleigh number increases, indicating that the dimensionless rate of mass transfer (or the convective flux, J_{conv}) of CO_2 into the brine at the interface decreases with increasing Rayleigh number.

Figure 11 plots the dimensionless flux rates of CO_2 at the interface, which are calculated from the slopes of the lines in Fig. 10. The following scaling relation is obtained:

$$J_{conv} = \frac{dm}{d\tau} = 0.0794 Ra^{-0.168}. \tag{30}$$

In Eq. 30, m_D and τ are dimensionless parameters. The dimensional mass-transfer rate increases with increasing Rayleigh number, because the maximum soluble mass of CO_2 increases with increasing Ra. Assuming

Fig. 11 The dimensionless convective flux of CO_2 at the interface as a function of Rayleigh number
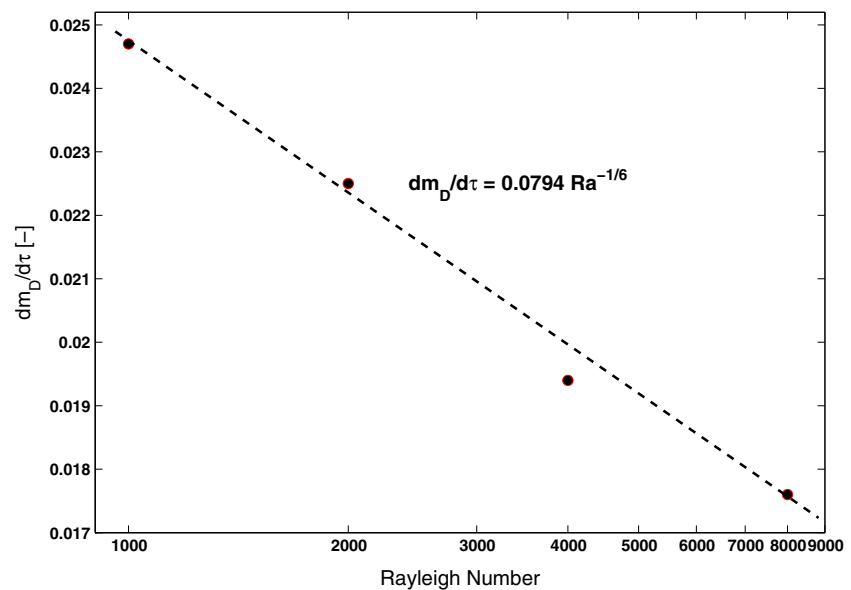
that Henry's law is valid at high pressures, the maximum soluble CO_2 is given by

$$m_{sat} = \frac{P_{CO_2} M_{CO_2} V_{CO_2}}{k_H}.$$

Using Eq. 31, the dimensional form of Eq. 30 becomes

$$j_{conv} = \frac{dm}{dt} = \kappa \, Ra^{5/6} \tag{31}$$

where

$$\kappa = 0.0794 M_{CO_2} \frac{D}{\varphi H^2} \left(\frac{P_{CO_2} V_{CO_2}}{k_H} \right)$$

$$= 0.0035 \frac{D}{\varphi H^2} \left(\frac{P_{CO_2} V_{CO_2}}{k_H} \right). \tag{32}$$

where P_{CO_2} is the pressure of gaseous CO_2, V_{CO_2} is the volume of the gaseous CO_2, k_H is Henry's solubility constant, and M_{CO_2} is the molecular weight of CO_2.

4 Conclusions

- Following a similar procedure to that proposed by [28], we developed an analytical model to predict transfer between the overriding carbon dioxide layer and the brine layer below it. The model is able to describe gravitationally unstable flow in porous media.
- The method of matched asymptotic expansions was used to obtain an approximate analytical solution for the relevant equations describing both the diffusive and convective regimes. The solution is characterized by a thin diffusive layer that separates the interface from a zone below where gravity unstable flow occurs.
- The developed model takes the gravity fingering index (or K_G factor) and a dilution factor, α_τ, as input parameters and provides the average concentration of CO_2 in the brine as a function of distance at different times.
- The solution of the convective part of the model starts at the saturation corresponding to the highest value of the fractional-flow function with a rarefaction solution at the downstream of the diffusive layer. Even if the agreement between the Koval solution and the numerical natural convection solution is only qualitative, it turns out that the transfer rate between the gas and liquid phase is adequately represented by the Koval model with two parameters. A reduced value of dilution factor α_τ can be attributed to mixing between fingers. However, the gravity fingering index K_G is purely empirical and has no obvious physical foundation.

- A comparison between the analytical model and the horizontally averaged concentrations obtained from 2-D numerical simulations provides a correlation for calculation of the K_G factor and the dilution factor, α_τ, for different Rayleigh numbers.
- The empirical relations between the K_G factor and the Rayleigh number, the dilution factor α_τ and the Rayleigh number, and the convective flux of CO_2 at the interface with Rayleigh number can be used in numerical simulators to account for the density-driven natural convection, which cannot be currently captured because the grid cells are typically orders of magnitude larger than the wavelength of the initial fingers.

References

1. Bando, S., Takemura, F., Nishio, M., Hihara, E., Makoto Akai, M.: Viscosity of aqueous NaCl solutions with dissolved CO_2 at (30 to 60) °C and (10 to 20) MPa. J. Chem. Eng. Data **49**, 1328–1332 (2004)
2. Bedrikovetsky, P., De Deus, J., Eurico Altoé, J.: Secondary migration of oil: analytical model. SPE 69411. In: 2001 SPE Latin American and Caribbean Petroleum Engineering Conference. Buenos Aires, Argentina, SPE (2001)
3. Blackwell, R.J., Rayne, I.R., Terry, W.M.: Factors influencing the efficiency of miscible displacement. Petrol. Trans., AIME **217**, 1–4 (1959)
4. Booth, R.J.S.: On the growth of the mixing zone in miscible viscous fingering. J. Fluid Mech. **655**, 527–539 (2010)
5. Booth, R.J.S.: Miscible flow through porous media. PhD dissertation, University of Oxford (2008)
6. Dake, L.P.: Fundamentals of Reservoir Engineering, p. 365. Elsevier, New York (1978)
7. Dake, L.P.: The Practice of Reservoir Engineering, pp. 370–371. Elsevier, New York (1994)
8. Dougherty, E.L.: Mathematical model of an unstable miscible displacement. SPE J. **3**, 155–163 (1963), SPE 509
9. Enick, R.M., Klara, S.M.: CO_2 solubility in water and brine under reservoir conditions. Chem. Eng. Commun. **90**(1), 23–33 (1990)
10. Ennis-King, J., Paterson, L.: Role of convective mixing in the long-term storage of carbon dioxide in deep saline aquifers. SPE J. **10**(4), 349 (2005)
11. Farajzadeh, R., Salimi, H., Zitha, P.L.J., Bruining, J.: Numerical simulation of density-driven natural convection in porous media with application for CO_2 injection projects. Int. J. Heat Mass Transfer **50**(25–26), 5054–5064 (2007a)
12. Farajzadeh, R., Barati, A., Delil, H.A., Bruining, J., Zitha, P.L.J.: Enhanced mass transfer of CO_2 into water and surfactant solutions. Pet. Sci. Technol. **25**(13), 1493–1511 (2007b)
13. Farajzadeh, R., Farshbaf Zinati, F., Zitha, P.L.J., Bruining, J.: Density-driven natural convection in dual layered and

anisotropic porous media with application for CO_2 injection projects. A40 ECMOR XI. 8–11 September 2008, 11th European Conference on the Mathematics of Oil Recovery. Bergen, Norway (2008)

14. Farajzadeh, R., Bruining, J., Zitha, P.L.J.: Enhanced mass transfer of CO_2 into water: experiment and modeling. Ind. Eng. Chem. Res. **48**(10), 4542–4455 (2009)

15. Farajzadeh, R., Meulenbroek, B., Bruining, J.: An analytical method for predicting the performance of gravitationally unstable flow in porous media. SPE 143420. Presented at SPE EUROPEC/EAGE Annual Conference and Exhibition, 23–26 May 2011a, Vienna, Austria (2011a)

16. Farajzadeh, R., Ranganathan, P., Zitha, P.L.J., Bruining, J.: The effect of heterogeneity on the character of density-driven natural convection of CO_2 overlying a brine layer. Adv. Water Resour. **34**(4), 327–339 (2011b)

17. Fayers, F.J.: An approximate model with physically interpretable parameters for representing miscible viscous fingering. SPE Reserv. Eng. **3**, 551–558 (1988)

18. Fayers, F.J., Newley, T.M.J.: Detailed validation of an empirical model for viscous fingering with gravity effects. SPE Reserv. Eng. **3**, 542–550 (1988)

19. Fayers, F.J., Blunt, M.J., Christie, M.A.: Comparisons of empirical viscous-fingering models and their calibration for heterogeneous problems. SPE Reserv. Eng. **7**(2), 195–203 (1992)

20. Gelhar, L.W.: Stochastic Subsurface Hydrology. 390 pp, ISBN 0138467676. Prentice Hall, Englewood Cliffs (1993)

21. Gmelin L.: Gmelin Handbuch der anorganischen Chemie, 8. Auflage. Kohlenstoff, Teil C3, Verbindungen, pp. 64–75 (1973)

22. Guo, T., Neale, G.H.: Effects of buoyancy forces on miscible liquid–liquid displacement processes in a porous medium. Powder Technol. **86**, 265–273 (1996)

23. Hassanzadeh, H., Pooladi-Darvish, M., Keith, D.: Scaling behavior of convective mixing, with application to CO_2 geological storage. AIChE J. **53**(6), 1121–1131 (2007)

24. Hearn, C.L.: Simulation of stratified waterflooding by pseudo relative permeability curves. JPT 805–13 (1971)

25. Hebach, A., Oberhof, A., Dahmen, N.: Density of water + carbon dioxide at elevated pressures: measurements and correlation. J. Chem. Eng. Data **49**(5), 950–953 (2004)

26. Hill, S.: Chanelling in packed columns. Chem. Eng. Sci. **1**, 247–253 (1952)

27. Khosrokhavar, R., Elsinga, G., Mojaddam, A., Farajzadeh, R., Bruining, J.: Visualization of natural convection flow of (sub-) and (super-) critical CO_2 in aqueous and oleic systems by applying Schlieren method. 73rd EAGE Conference and Exhibition Incorporating SPE EUROPEC 2011, SPE 143264 (2011)

28. Koval, E.J.: A method for predicting the performance of unstable miscible displacement in heterogeneous media. SPE J. **3**(2), 145–154 (1963)

29. Kumagai, A., Yokoyama, C.: Viscosities of aqueous NaCl solutions containing CO_2 at high pressures. J. Chem. Eng. Data **44**, 227–229 (1999)

30. Lake, L.W.: Enhanced Oil Recovery. Prentice Hall, Englewood Cliffs (1989)

31. Landau, L.D., Lifshitz, E.M.: Course of theoretical physics. Fluid Mechanics. Series in Advanced Physics, vol. 6. Addison-Wesley, Reading (1959)

32. Lu, C., Lichtner, P.C.: High resolution numerical investigation on the effect of convective instability on long-term CO_2 storage in saline aquifers. J. Phys.: Conf. Ser. **78**, 12042 (2007)

33. Neufeld, J.A., Hesse, M.A., Riaz, A., Hallworth, M.A., Tchelepi, H.A., Huppert, H.E.: Convective dissolution of carbon dioxide in saline aquifers. Geophys. Res. Lett. **37**(23) (2010) art. no. L22404

34. Pau, G.S.H., Bell, J.B., Pruess, K., Almgren, A.S., Lijewski, M.J., Zhang, K.: High-resolution simulation and characterization of density-driven flow in CO_2 storage in saline aquifers. Adv. Water Resour. **33**(5), 443–455 (2010)

35. Peaceman, D.W., Rachford Jr., H.H.: Numerical calculation of multi-dimensional miscible displacement. Soc. Pet. Eng. J. **2**, 327–339 (1962)

36. Perrine, R. L. : The development of stability theory for miscible liquid–liquid displacement. Soc. Pet. Eng. J. **1**(1), 17–25 (1961)

37. Ranganathan, P., Farajzadeh, R., Bruining, J., Zitha, P.L.J.: Numerical simulation of natural convection in heterogeneous porous media for CO_2 geological storage. Transp. Porous Med. **95**, 25–54 (2012)

38. Riaz, A., Tchelepi, H.A.: Dynamics of vertical displacement in porous media associated with CO_2 sequestration. Proceedings of the SPE Annual Technical Conference and Exhibition 6, pp. 4298–309 (2006)

39. Riaz, A., Hesse, M., Tchelepi, A., Orr, F.M.: Onset of convection in a gravitationally unstable diffusive boundary layer in porous medium. J. Fluid Mech. **548**, 87–111 (2006b)

40. Siddiqui, F.I., Lake, L.W.: A comprehensive dynamic theory of hydrocarbon migration and trapping. SPE 38682. In: 1997 72nd Annual Technical Conference and Exhibition, San Antonio, TX, SPE (1997)

41. Silin, D., Patzek, T., Benson, S.M.: A model of buoyancy-driven two-phase countercurrent fluid flow. Transp. Porous Med. **76**, 449–469 (2009)

42. Sharp, D.H.: An overview of Rayleigh–Taylor instability. Physica **12**D, 3–18 (1984)

43. Taylor, G.I.: The instability of liquid surfaces when accelerated in a direction perpendicular to their planes. Proc. R. Soc. Lond., A **201**, 192–196 (1950)

44. Todd, M.R., Longstaff, W.J.: The development, testing, and application of a numerical simulator for predicting miscible flood performance. J. Pet. Technol. **24**, 874–882 (1972)

45. Van Dyke, M.: Perturbation Methods in Fluid Mechanics. The Parabolic Press, Stanford (1975)

46. Verhulst, F.: Methods and Applications of Singular Perturbations. Springer, New York (2000)

47. Waggoner, J.R., Zapata, V.J., Lake, L.W.: Viscous mixing in unstable miscible displacements. SPE 22235-MS (1991)

48. Waggoner, J.R., Castillo, J.L., Lake, L.W.: Simulation of EOR processes in stochastically generated permeable media. SPE Form. Eval. **7**(2), 173–180 (1992)

49. Willhite, P.G.: Waterflooding, pp. 151–153. Society of Petroleum Engineers Inc., Richardson (1986), SPE textbook series

50. Wooding, R.A.: Growth of fingers at an unstable diffusing interface in a porous medium or Hele–Shaw cell. J. Fluid Mech. **39**, 477–495 (1969)

51. Yang, C., Gu, Y.: Accelerated mass transfer of CO_2 in reservoir brine due to density-driven natural convection at high pressures and elevated temperatures. Ind. Eng. Chem. Res. **45**, 2430–2436 (2006)

52. Yortsos, Y.C., Salin, D.: On the selection principle for viscous fingering in porous media. J. Fluid Mech. **557**, 225–236 (2006)

53. Zimmerman, W.B., Homsy, G.M.: Viscous fingering in miscible displacements: Unification of effects of viscosity contrast, anisotropic dispersion, and velocity dependence of dispersion on nonlinear finger propagation. Phys. Fluid A **4**, 2348–2359 (1992)